Received 22 April 2020; revised 24 May 2020; accepted 29 May 2020. Date of publication 3 June 2020; date of current version 18 June 2020.

Digital Object Identifier 10.1109/OJAP.2020.2999657

A Generalized Transition Matrix Model Combined With Discontinuous Galerkin Method for Open Cavities

YUYANG HU [1] (Graduate Student Member, IEEE), GAOBIAO XIAO [1] (Member, IEEE), AND SHANG XIANG [2] (Member, IEEE)

[1]Key Laboratory of Ministry of Education of Design and Electromagnetic Compatibility of High-Speed Electronic Systems, Shanghai Jiao Tong University, Shanghai 200240, China

[2]Department of Electrical and Information Technology, Lund University, 22100 Lund, Sweden

CORRESPONDING AUTHOR: G. XIAO (e-mail: gaobiaoxiao@sjtu.edu.cn)

This work was supported in part by the National Key Research and Development Program of China under Grant 2019YFB2204703, and in part by the Guangdong Provincial Key-Field Research Program under Grant 2018B010115001.

ABSTRACT A generalized transition matrix (GTM) model combined with discontinuous Galerkin (DG) method is proposed to analyze the scattering problems of open-ended cavities. A virtual reference surface is put to seal the opening of an open cavity and can separate it into an exterior region and an interior region. By mapping the scattering properties of the internal components onto the reference surface, the information interaction of the GTM model occurs on the reference surface only. With its features of nonconformal meshes at the boundary, the DG method makes the model feasible and accurate regardless of the normal continuity of the surface current at the transitional interface. The GTM model is independent of the exterior structure of the cavity and the external fields. The computational cost can be significantly decreased when the GTM model with the identical inner region is reused. Numerical examples demonstrate good precision and efficiency of the presented method.

INDEX TERMS Generalized transition matrix (GTM), discontinuous Galerkin (DG), open cavity, reference surface.

I. INTRODUCTION

THE ANALYSIS of electromagnetic scattering properties of open-ended cavities has recently obtained a lot of attentions due to the importance of radar cross-section (RCS) problems. Open-ended metal cavities are widely applied in electronic components, packaging technology and electromagnetic protection, such as arrays with a dielectric resonator antenna (DRA) embedded in the open metallic cavity [1], the cavity diplexer [2], and the coplanar stripline with a metal shielding cavity [3]. To determine the resonator modes of DRA configuration, both the radiation fields and the scattering fields are necessary to be considered. Therefore, a highly efficient numerical method for calculating the electromagnetic properties of open cavities with complex interior structures deserves consideration.

Traditional numerical methods such as the method of moment (MoM) [4], [5] and the finite element method (FEM) [6] have been used to accurately analyze open cavities. Nevertheless, such methods are very time-consuming when fine internal structures are set inside the cavity. Some hybrid numerical methods have been studied, such as physical optics-finite difference time domain [7], and hybrid FEM [8], to analyze the scattering by tracking the fields from the cavity through modal techniques applying a relevant generalized scattering matrix. A multi-method and multi-domain coupling strategy based on generalized scattering matrix calculations in subdomains is developed in [9]. The generalized scattering matrix is calculated by various methods like FEM or the electric field integral equation (EFIE) in each subdomain. But the application in multi-cavities system is not considered in these methods. A radiation computation scheme based on the field sampling in an open slot on the surface of the shielded box is applied to model the radiation fields from the printed circuit

board (PCB) inside the box [10], however, the coupling effect from the external field on the internal circuit is ignored. The finite element boundary integral method is presented to solve scattering problems for cavities in [11], [12]. The equivalence principle algorithm for domain decomposition is introduced in the case where the equivalence surfaces intercept with current-carrying metallic structures [13].

In our previous work [14], a generalized transition matrix (GTM) model [15] based on the equivalence principle has been presented to capture the electromagnetic properties of an open-ended cavity with interior composition. However, the currents flowing across the junctions are defined by conventional Rao-Wilton-Glisson (RWG) basis functions [16]. It is required to extend surface currents to nearby regions of the junctions to make the meshes matching across the junctions, which is inconvenient in practical application. For example, when the exterior surface of the cavity changes to an irregular shape or the thickness of the wall is less than the height of the triangle mesh at the transitional junctions, it is required to adjust the meshes there. Otherwise, the GTM model in [14] needs to be recalculated, losing its advantage.

To overcome the discontinuity of the approximation, the discontinuous Galerkin (DG) method presents a very appealing possibility [17]. DG method supports a variety of types and shapes of elements and nonconformal meshes because the normal continuity is weakly satisfied and the discontinuity is allowed across the boundary contours. Generally, the DG method is applied with surface integral equations (SIE) [18] expressed by introducing an interior penalty (IP) term as in [19]. Different from it, an intuitive formulation is proposed in [20], which is constructed by performing singularity extraction and removing infinite terms. The concept of domain decomposition method (DDM) has been embedded into the DG method recently and successfully applied for solving scattering problems with SIE [21], [22]. DG methods based on DDM are widely used for PEC targets [22], homogeneous objects [23] and targets with impedance boundary conditions (IBCs) [24].

In this paper, we propose a novel GTM method combined with DG method to represent the properties of fine interior ingredients of the cavity. Instead of surrounding the scatterer with a completely global surface as suggested in [15], a local virtual reference surface is set to close the windows or openings on the cavity and partition the cavity into the exterior region and interior region. The two regions can be meshed separately. The reference surface and the internal ingredients are considered as a whole and can be solved with conventional SIEs with RWGs. The exterior region encompassing the outer wall is treated as the background. The DG method is applied to deal with the boundary of junctions rather than conventional RWG basis functions. Different from [14], the reference surface and the external wall of the target cavity form two nonoverlapping sub-surfaces, and the meshes along the junctions can be nonconformal. Along the interfaces between the outer wall and the reference surface, we discretize the surface currents with

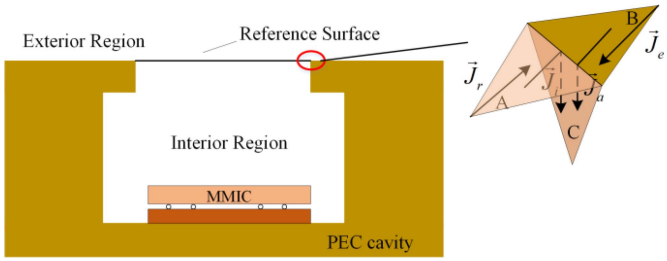

FIGURE 1. An equivalent GTM model of the cavity.

half RWG (HRWG) basis functions [19] while using RWG basis functions inside each sub-surface. A relevant GTM model is obtained by capturing the scattering and radiation information of the interior region onto the reference surface. As long as the opening and the interior structure remain identical, the GTM model is fixed and no recalculation is required no matter how the exterior environment changes, so that it can be freely applied to periodic structure cavity without the necessity to ensure the mesh matching at the interface, thus maintaining the robustness of the GTM method. In general, the newly proposed GTM model is more flexible and more robust than the method in [14]. The size of the obtained GTM model is dependent on the number of unknowns of equivalent currents on the reference surface only. Especially when the interior region contains complicated ingredients with fine meshes, the computational cost can be significantly diminished.

This paper is organized as follows. Section II introduces the methodology of the DG method and the derivation of the GTM algorithm. Some numerical experiments are shown to validate the advantages of the presented method in Section III. Finally, some conclusions are drawn in Section IV.

II. METHODOLOGY OF THE GTM MODEL FOR OPEN CAVITIES

A. REFERENCE SURFACE—CAVITY JUNCTION

Consider that a monolithic microwave integrated circuit (MMIC) is set in the cavity. Once the structure of MMIC contains many details, analyzing the scattering characteristics with the conventional MoM becomes quite inefficient. Hence, an equivalent reference surface is placed to close the opening of the cavity plotted in Fig. 1, which strictly divides the cavity into two parts: exterior region and interior region. Since the reference surface is not a perfect electric conductor (PEC), the presence of electric and magnetic currents is allowed. According to the Huygens principle, the external excitation field interacts with the scattering field inside the cavity via the reference surface.

The reference surface seals the windows of the target cavity, which means that it cuts off the electric currents from the exterior wall to the interior wall of the cavity. However, the surface electric currents must be subject to the continuity law at the junction. Therefore, we should pay more attention to find an effective method to discretize the electric currents

on the external surface and internal surface respectively and keep the electric currents on the actual junction of the cavity continuous.

We present to discretize the surface currents at the exterior interface by HRWG basis function and still use the RWG basis function at the interior interface. In Fig. 1, we introduce four basis electric currents $\vec{J}_a$, $\vec{J}_r$, $\vec{J}_e$ and $\vec{J}_i$ at the junction, where triangle-A, triangle-B, and triangle-C are respectively at the reference surface, the external surface and the internal surface of the cavity. $\vec{J}_a$ is an RWG basis current and denotes the actual currents flowing from the external surface to the internal surface of the cavity. $\vec{J}_r$ and $\vec{J}_e$ are HRWG basis currents and represent the currents at the jagged part of the contour on the reference surface and the external surface of the cavity, respectively. $\vec{J}_i$ is RWG-typed current and stands for the currents from reference surface to internal surface of the cavity. In the case of the conformal meshes, we have

$$\vec{J}_a = \vec{J}_r + \vec{J}_e + \vec{J}_i \tag{1}$$

There are no magnetic currents on the surface of the metallic cavity. Hence no magnetic currents flow across the junction correspondingly and the boundary conditions at the junction are similar to the conditions of PEC structures. It should be noted that these bounding triangles, like triangle-A, are regarded as PEC materials only when tested by these junction basis functions. When tested by other basis functions, they are not treated as PECs.

B. DG METHOD

The DG method based on a non-overlapping, nonconformal DDM is applied to keep the normal weak continuity of the boundary contours between the exterior surface and the reference surface. The exterior wall of the cavity and the reference surface constitute two different subdomains, where RWGs are expanded on the internal edges inside subdomains and HRWGs are defined on the contour between subdomains, as plotted in Fig. 2. Note that the triangle meshes at the interface between subdomains are not strictly bound to be conformal, nonconformal meshes are also feasible which make it possible to control the density of meshes in different regions. The total current on the outside of the reference surface is expanded by hybrid basis functions.

$$J(\vec{r}) = \vec{J}_R + \vec{J}_H = \sum_{m=1}^{N_R} j_m^R f_m^R(\vec{r}) + \sum_{m=1}^{N_H} j_n^H f_n^H(\vec{r}) \tag{2}$$

where $f_m^R(\vec{r}), m = 1, \ldots, N_R$ and $f_n^H(\vec{r}), n = 1, \ldots, N_H$ are RWGs and HRWGs. N_R and N_H are the number of RWGs and HRWGs, respectively. More details about HRWG basis functions can be found in [19].

In the GTM model, the radiation field contributed by the current $\vec{J}_e$ is a part of the incident fields for the cavity. In this case, we need to calculate the coefficients of the current $\vec{J}_e$ so that we encounter the noticeable line-line integral. When the reference lines of two triangles at the boundary between subdomains do not coincide, line-line integral

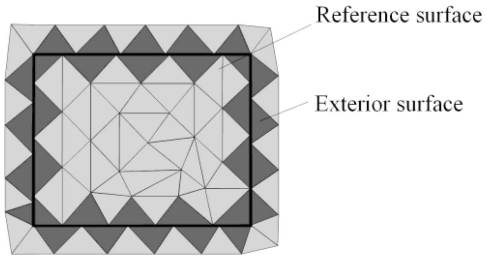

FIGURE 2. Half RWG basis functions are defined along the interface contour (darker gray area) and RWG basis functions are define inside the subdomains (lighter gray area).

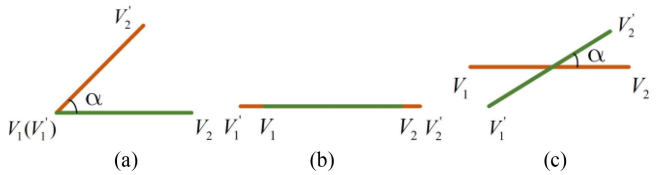

FIGURE 3. The coincidence relationship of line segments. (a) Adjacent vertex. (b) Overlapping edges. (c) Intersection.

can be accurately calculated using Gaussian numerical integration. However, when the reference lines coincide at the contour, accumulation of charge leads to the infinite and singular line-line integral in mutual coupling or self-coupling. Singularity occurs in vertex adjacency, the overlap between edges and intersection. The coincidence relationship of line segments is shown in Fig. 3. The coplanar intersection between edges can be transformed into vertex adjacency. When the intersection is faceted, we can apply local coordinate with the origin locating at one foot of the common perpendicular line. Therefore, line-line integral in the case of coincidence can be converted into two basic forms: integral of adjacent vertex and overlapping edges. We apply the strategy of coordinate transformation and eliminating the integral domain singular interval Δ [20] to calculate limited line-line integrals.

The distance between the field point and source point is represented as $R = |\vec{r} - \vec{r}'|$. Besides, we define that $l_1 = |\overrightarrow{V_1 V_2}|$ and $l_2 = |\overrightarrow{V_1' V_2'}|$ represent the length of the reference line in testing basis function $f_m^R(\vec{r})$ and source basis function $f_n^H(\vec{r}')$. The Green's function in line-line integral can be decomposed into

$$\int_{L_m}\int_{L_n'} \frac{e^{-jkR}-1}{4\pi R} dL' dL + \int_{L_m}\int_{L_n'} \frac{1}{4\pi R} dL' dL \tag{3}$$

where k denotes the wavenumber. The first term at the right side of (3) is non-singular and can be solved by traditional Gaussian numerical integration.

Consider the line-line integral of adjacent vertex, point V_1 and V_1' coincide, which means that the vertex V_1 is both an observation point and source point, so that the second term of (3) is singular. Denote $l_3 = |\overrightarrow{V_2 V_2'}|$. By transforming the coordinate, the second term can be explicitly

evaluated as

$$I_1 = \int_{L_m}\int_{L_n'} \frac{1}{R} dL' dL = l_1 \ln \frac{l_2 + l_3 - l_1 \cos\alpha}{l_1(1-\cos\alpha)} + l_2 \ln \frac{l_1 + l_3 - l_2 \cos\alpha}{l_2(1-\cos\alpha)} \tag{4}$$

where the singularity of line-line integral is canceled out.

As for the line-line integral of the overlapping edge, we remove the infinitely small area Δ near the singular points. In this way, the line-line integral is bounded. The line integral I_1 can be rewritten as

$$I_1 \approx 2l_1(\Delta - \ln\Delta - 1) \tag{5}$$

where we have $\lim_{\Delta\to 0}(\Delta - \ln\Delta - 1) = \infty$. Δ can be treated as a loosen coefficient that converts the infinitely large double contour integral into bounded integral. By controlling the value of Δ, the local numerical precision of the singular integral can be controlled.

Since all the singular line-line integral can be transformed into the above two basic forms, the singularity is picked out analytically. Decomposing and meshing the curved surfaces separately inevitably lead to gaps, overlaps or intersections. But the proposed DG method can still analyze these situations directly, so that it provides great convenience for mesh generation and local densification by appropriately loosening the continuity along the boundary between subdomains.

C. FORMULATION DERIVATION OF GTM

To simplify the derivation of the GTM method, a simple metallic cavity is shown in Fig. 4, where a virtual reference surface is placed to close the opening of the cavity. Apart from the preceding work [25], a scattering source $\vec{I}_s$ is added inside the cavity to indicate the presence of the internal source. Equivalent electric and magnetic currents flow on the reference surface, according to the equivalence theorem. In Fig. 4, $\vec{E}^{inc}$ and $\vec{H}^{inc}$ indicate the natural incident wave. $\vec{J}_R^{ex}$ and $\vec{M}_R^{ex}$ on the outside plane of the reference surface S_R, and $\vec{J}_R^{in}$ and $\vec{M}_R^{in}$ on the inside plane of the reference surface S_R make contributions to the fields in the external and internal region separately. Due to the metal surface of the cavity, there are also inductive currents on the exterior wall S_{ex} and interior wall S_{in}, which are represented by $\vec{J}_W^{ex}$ and $\vec{J}_W^{in}$. The current $\vec{J}_e$ from the exterior wall to the reference surface, and the current $\vec{J}_r$ from the reference surface to the exterior wall, indicate currents at the external transitional interface. The current $\vec{J}_i$ exists from the reference surface to the interior wall at the internal interface. The processing of three currents at the junction has been mentioned in the previous subsection. The rest electric and magnetic currents are discretized by RWGs. In the subsequent derivation, we use $\vec{J}_{in}$ to represent the combined current of $\vec{J}_i$ and $\vec{J}_W^{in}$. Furthermore, currents $\vec{J}_R^{ex/in}$ and $\vec{M}_R^{ex/in}$ exist only on the reference surface and magnetic current does not flow across the boundary of the reference surface.

According to the equivalent principle, when the observation points are outside the cavity, the total electromagnetic field contributed by equivalent electric and magnetic currents can be denoted as following integral equations:

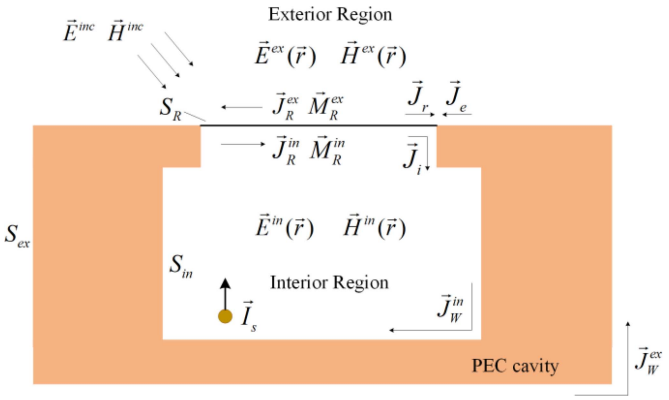

FIGURE 4. A PEC cavity for the formula derivation.

$$\vec{E}^{ex}(\vec{r}) = \eta_{ex}\mathcal{L}_{ex}\left(\vec{J}_R^{ex}\right) - \mathcal{K}_{ex}\left(\vec{M}_R^{ex}\right) + \eta_{ex}\mathcal{L}_{ex}\left(\vec{J}_W^{ex}\right) + \eta_{ex}\mathcal{L}_{ex}\left(\vec{J}_e\right) + \eta_{ex}\mathcal{L}_{ex}\left(\vec{J}_r\right) + \vec{E}^{inc} \tag{6}$$

$$\vec{H}^{ex}(\vec{r}) = \frac{1}{\eta_{ex}}\mathcal{L}_{ex}\left(\vec{M}_R^{ex}\right) + \mathcal{K}_{ex}\left(\vec{J}_R^{ex}\right) + \mathcal{K}_{ex}\left(\vec{J}_W^{ex}\right) + \mathcal{K}_{ex}\left(\vec{J}_e\right) + \mathcal{K}_{ex}\left(\vec{J}_r\right) + \vec{H}^{inc} \tag{7}$$

When the observation points are set inside the cavity, the total electromagnetic field can be described as:

$$\vec{E}^{in}(\vec{r}) = \eta_{in}\mathcal{L}_{in}\left(\vec{J}_R^{in}\right) - \mathcal{K}_{in}\left(\vec{M}_R^{in}\right) + \eta_{in}\mathcal{L}_{in}\left(\vec{J}_{in}\right) + \eta_{in}\mathcal{L}_{in}\left(\vec{I}_s\right) \tag{8}$$

$$\vec{H}^{in}(\vec{r}) = \frac{1}{\eta_{in}}\mathcal{L}_{in}\left(\vec{M}_R^{in}\right) + \mathcal{K}_{in}\left(\vec{J}_R^{in}\right) + \mathcal{K}_{in}\left(\vec{J}_{in}\right) + \mathcal{K}_{in}\left(\vec{I}_s\right) \tag{9}$$

where η represents the intrinsic impedance and the subscripts indicate the exterior and interior regions. The two operators $\mathcal{L}$ and $\mathcal{K}$ are written as:

$$\mathcal{L}_i\left(\vec{X}\right) = -jk_i \int_S \left[\vec{X} + \frac{1}{k_i^2}\nabla\left(\nabla' \bullet \vec{X}\right)\right] G_i(\vec{r},\vec{r}')dS' \tag{10}$$

$$\mathcal{K}_i\left(\vec{X}\right) = -\int_S \vec{X} \times \nabla\, G_i(\vec{r},\vec{r}')dS' \tag{11}$$

where subscript i denotes the exterior or interior regions of the cavity. $G_i(\vec{r},\vec{r}')$ represents the space Green's function of the different areas. k_i is the space wave number.

Consider that the background medium of exterior and interior regions is free space so that we can easily obtain $\vec{J}_R^{ex} = -\vec{J}_R^{in}$ and $\vec{M}_R^{ex} = -\vec{M}_R^{in}$. We define $\vec{J}_R^{ex} = \vec{J}_R$ and $\vec{M}_R^{ex} = \vec{M}_R$. In this way, operators $\mathcal{L}_i$ and $\mathcal{K}_i$ can be unified into operators $\mathcal{L}$ and $\mathcal{K}$. η_{ex} and η_{in} are replaced by η, and k_i is rewritten by k as well in the following derivation.

The tangential components of the electromagnetic fields in the interior and exterior regions meet the boundary continuity conditions. Therefore, on the reference surface, the set of

equations can be constructed as:

$$\left[-2\eta\mathcal{L}\left(\vec{J}_R\right)+2\mathcal{K}\left(\vec{M}_R\right)+\eta\mathcal{L}\left(\vec{J}_{in}\right)+\eta\mathcal{L}\left(\vec{I}_s\right)\right]|_{\tan}$$
$$=\left[\eta\mathcal{L}\left(\vec{J}_W^{ex}\right)+\eta\mathcal{L}\left(\vec{J}_e\right)+\eta\mathcal{L}\left(\vec{J}_r\right)+\vec{E}^{inc}\right]|_{\tan},\ \forall\vec{r}\in S_R \quad (12)$$

$$\left[-\frac{2}{\eta}\mathcal{L}\left(\vec{M}_R\right)-2\mathcal{K}\left(\vec{J}_R\right)+\mathcal{K}\left(\vec{J}_{in}\right)+\mathcal{K}\left(\vec{I}_s\right)\right]|_{\tan}$$
$$=\left[\mathcal{K}\left(\vec{J}_W^{ex}\right)+\mathcal{K}\left(\vec{J}_e\right)+\mathcal{K}\left(\vec{J}_r\right)+\vec{H}^{inc}\right]|_{\tan},\ \forall\vec{r}\in S_R \quad (13)$$

Then the RWGs on the reference surface are selected as testing basis function so that the equations (12) and (13) can be transformed into the matrix form:

$$\mathbf{Z}_R\bullet\mathbf{X}_R^-+\mathbf{A}\bullet\mathbf{J}_{in}+\mathbf{D}\bullet\mathbf{I}_s=\mathbf{X}_R^++\mathbf{Z}_r\bullet\mathbf{J}_r \quad (14)$$

where $\mathbf{X}_R^-$ consists of the expansion coefficient of $\vec{J}_R$ and $\vec{M}_R$ that are the rotated tangential components of the scattering magnetic field and electric field on the reference surface. $\mathbf{X}_R^+$ indicates the tangential components of the total incident fields, which include the scattering from the outer wall of the cavity and the external excitation. $\mathbf{J}_{in}$ denotes the expansion coefficient of the current on the interior surface including the inner junctions. $\mathbf{J}_r$ expresses the expansion coefficient of the current that is discretized by the HRWGs on the sawtooth portion of the reference surface. $\mathbf{Z}_R$ represents the self-impedance matrix of the reference surface. $\mathbf{A}$ stands for the coupling matrix between the reference surface and the interior wall. $\mathbf{D}$ represents the field transmission matrix onto the reference surface contributed by an internal source $\mathbf{I}_s$. Besides, the matrix $\mathbf{Z}_r$ indicates the coupling matrix between the reference surface and the jagged part of the edge on the reference surface. The DG method is applied here to keep the weak current continuous on the border. The matrix $\mathbf{Z}_r$ can be represented as:

$$(\mathbf{Z}_r)_{i,j}=\begin{bmatrix}\mathbf{Z}_{i,j}^{ERH}\\ \mathbf{Z}_{i,j}^{MRH}\end{bmatrix} \quad (15)$$

The elements of the matrix can be written into:

$$\mathbf{Z}_{i,j}^{ERH}=-j\omega\mu_0\int_{S_m}\vec{f}_m^{Ri}(\vec{r})\cdot\int_{S_n'}\vec{f}_n^{Hj}(\vec{r}')G_0(\vec{r},\vec{r}')dS'dS$$
$$-\frac{1}{j\omega\varepsilon_0}\int_{S_m}\nabla_s\cdot\vec{f}_m^{Ri}(\vec{r})\int_{S_n'}\nabla_s'\cdot\vec{f}_n^{Hj}(\vec{r}')G_0(\vec{r},\vec{r}')dS'dS$$
$$+\frac{1}{j\omega\varepsilon_0}\int_{S_m}\nabla_s\cdot\vec{f}_m^{Ri}(\vec{r})\int_{L_n'}\vec{t}_n^{Hj}\cdot\vec{f}_n^{Hj}(\vec{r}')G_0(\vec{r},\vec{r}')dL'dS \quad (16)$$

$$\mathbf{Z}_{i,j}^{MRH}=-\int_{S_m}\vec{f}_m^{Ri}(\vec{r})\cdot\int_{L_n'}\vec{f}_n^{Hj}(\vec{r}')\times\nabla G_0(\vec{r},\vec{r}')dL'dS \quad (17)$$

where μ_0 and ε_0 stand for the permeability and the permittivity in the free space separately. $\vec{t}_n$ indicates the unit normal vector on the boundary contour L_n.

As for the inner metallic surface of the cavity, according to the boundary conditions of PECs, the electric field integral equation is expressed as:

$$\left[\eta\mathcal{L}\left(\vec{J}_R\right)-\mathcal{K}(\vec{M}_R)-\eta\mathcal{L}\left(\vec{J}_{in}\right)-\eta\mathcal{L}\left(\vec{I}_s\right)\right]|_{\tan}=0,\ \forall\vec{r}\in S_{PEC}^{in} \quad (18)$$

After the testing procedure by the RWGs on the interior surface, the formula (18) can be converted into:

$$\mathbf{C}\bullet\mathbf{X}_R^-+\mathbf{B}\bullet\mathbf{J}_{in}+\mathbf{E}\bullet\mathbf{I}_s=0 \quad (19)$$

where $\mathbf{B}$ expresses the self-impedance matrix of the interior metal surface including the internal interface. $\mathbf{C}$ represents the coupling matrix between the interior surface and the reference surface. Similarly, $\mathbf{E}$ denotes the field transmission matrix from the internal source $\mathbf{I}_s$ to the interior surface.

To eliminate current coefficients $\mathbf{J}_{in}$ by substituting (19) into (14), the GTM model of the open-end cavity can be represented as:

$$\mathbf{X}_R^-=\mathbf{T}\bullet\mathbf{X}_R^++\mathbf{M}\bullet\mathbf{J}_r+\mathbf{N}\bullet\mathbf{I}_s \quad (20)$$

The reference surface is constructed by N_R RWGs and N_H HRWGs. The current at the interior interface is discretized by N_H RWGs as well. In this way, the $2N_R\times 2N_R$ matrix $\mathbf{T}$ is defined as GTM, which is applied to denote the responses to the total tangential incident fields on the reference surface. And the $2N_R\times N_H$ matrix $\mathbf{M}$ stands for the scattering fields contributed by the current $\vec{J}_r$. The $2N_R\times 1$ matrix $\mathbf{N}$ denotes the mapping matrix from the internal excitation to the reference surface. When there are N_i sources inside the cavity, $\mathbf{N}$ is a $2N_R\times N_i$ matrix.

The scattering fields of the GTM model include three parts: the responses to the total tangential incident fields on the reference surface, the generating from the current at the sawtooth portion of the boundary on the reference surface, and the mapping from radiating fields of internal excitations to reference surface. The matrices $\mathbf{T}$, $\mathbf{M}$ and $\mathbf{N}$ only depend on the internal ingredients and the reference surface. Their dimension is determined by the meshes on the reference surface only. Therefore, the size of the GTM can be much smaller than the size of the interior components, especially when the complicated internal compositions are put in the cavity.

The GTM model can describe the radiation and scattering properties of the cavity with complicated structures, such as DRA, MMIC, and multi-stack chips, and make the information interact only on the reference surface. Moreover, as long as the interior structures keep fixed, the GTM model can be conveniently transplanted no matter how the exterior environment transforms, which can significantly reduce the computational cost.

D. GTM MODELS OF MULTI-CAVITIES SYSTEM

Consider a complex array system consisting of multiple open cavities with fine interior structures. The individual cavity can be independently constructed as a GTM model. In this way, when analyzing the scattering characteristics of a specific cavity, radiation from other cavities can be considered as a part of the incident field. The complex system is simplified in Fig. 5. M open cavities are exposed to external surroundings. The reference surfaces are set to completely seal the apertures on all cavities and respectively extract

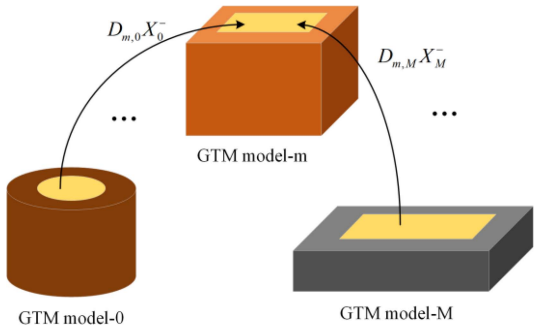

FIGURE 5. GTM models of the multi-cavities system.

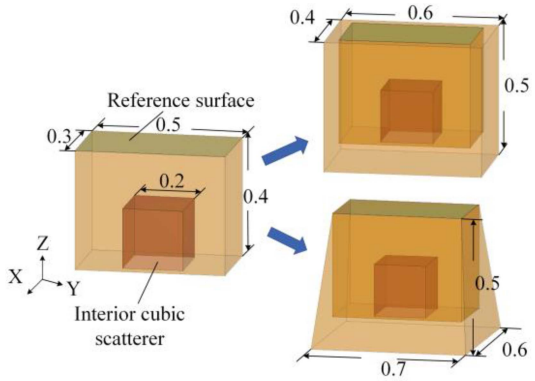

FIGURE 6. Identical interior cubic scatterer inside different outer surfaces.

the GTM models. The coupling between different cavities is transformed into the mutual coupling between GTM models. $\mathbf{X}_m^-$ indicates the rotated tangential components of the scattering field of the cavity m on the reference surface. In addition, the field transmission matrix $\mathbf{D}_{mn}$ is applied to denote the coupling influence between GTM model-m and GTM model-n, which is introduced in detail in [15].

Taking the cavity m in Fig. 5 as an example, the tangential components of the whole incident fields on the relevant reference surface can be described as:

$$\mathbf{X}_m^+ = \sum_{n=1,n\neq m}^{M} \mathbf{D}_{mn} \bullet \mathbf{X}_n^- + \mathbf{D}_{m0} \bullet \mathbf{J}_0 + \sum_{n=1}^{M} \mathbf{D}_{me}^n \bullet \mathbf{J}_e^n + \sum_{n=1,n\neq m}^{M} \mathbf{D}_{mr}^n \bullet \mathbf{J}_r^n + X_m^{inc} \tag{21}$$

where $\mathbf{D}_{m0}$ represents the field coupling between the reference surface of the GTM model-m and the exterior metallic surfaces of the cavities excluding the outer interfaces. $\mathbf{J}_0$ denotes the set of expansion coefficients of the induced current on the exterior metal wall of all the cavities in the complex system, which do not contain the current at the outer interfaces. $\mathbf{D}_{me}\mathbf{J}_e$ and $\mathbf{D}_{mr}\mathbf{J}_r$ stand for the fields generated by current $\mathbf{J}_e$ and $\mathbf{J}_r$ mapped onto the reference surface. $\mathbf{X}_m^{inc}$ represents the incident electromagnetic wave of the natural excitation. In a word, the total incident fields for a single GTM model come from the scattering fields of other GTM models, the electromagnetic field from each interface and the outer wall of the cavity, and the external excitation.

In the exterior region of the multi-cavities system, the total electric fields devoted by the total electric and magnetic currents can be described as:

$$\vec{E}_{total}^{ex}(\vec{r}) = \sum_{m=1}^{M}\left(\eta\mathcal{L}\left(\vec{J}_{m,R}^{ex}\right) - \mathcal{K}\left(\vec{M}_{m,R}^{ex}\right)\right) + \eta\mathcal{L}\left(\vec{J}_0\right) + \sum_{m=1}^{M}\eta\mathcal{L}\left(\vec{J}_{m,e}\right) + \sum_{m=1}^{M}\eta\mathcal{L}\left(\vec{J}_{m,r}\right) + \vec{E}^{inc} \tag{22}$$

On the outer surface S_{PEC}^{ex} and the jagged parts at all interfaces S_{PEC}^{e} and S_{PEC}^{r}, the equation is established according to the boundary condition of PECs:

$$\vec{E}_{total}^{ex}(\vec{r})|_{\tan} = 0, \ \forall \vec{r} \in S_{PEC}^{ex} \ or \ S_{PEC}^{e} \ or \ S_{PEC}^{r} \tag{23}$$

Choosing the RWGs on the S_{PEC}^{ex}, and the HRWGs on the S_{PEC}^{e} and S_{PEC}^{r} as the testing basis functions separately, we can obtain all matrix forms of $\vec{J}_0$, $\vec{J}_e$ and $\vec{J}_r$. By solving these matrix forms with (20), (21) concurrently, we can calculate the whole rotated tangential components of the scattering magnetic field and electric field on each reference surface, and the expansion coefficients of the currents on the exterior surfaces of multi-cavities. Then all current distributions in the system can be obtainable. Compared with the MoM when the complex compositions are inside the cavity and discretized by meticulous meshes, the dimension of the GTM model representing the electromagnetic characteristic of the internal region depends on the meshes of the GTM reference surfaces only, so that it can be much smaller than the size of the internal structure. Hence, the number of unknowns in the complex system can be obviously decreased. Especially for the problem of the periodic cavity arrays system where the interior region of each cavity is identical, the GTM model only needs to be calculated once and can be reused for remaining cavity arrays to characterize the scattering of internal structures. In the process of reusing, it is not necessary to concern about the mesh discretization at the interface, contributed by the DG method. In this way, calculating the scattering of complex periodic cavity systems becomes simple and convenient.

III. NUMERICAL RESULTS

Several numerical examples are described to demonstrate the efficiency and feasibility of the proposed GTM method in this section.

A. CAVITY WITH INTERIOR SCATTERER

In the following, the scattering of a PEC cavity with an internal cubic metallic scatterer is analyzed. The GTM model can be reused no matter how the external environment varies, as long as the interior composition of the cavity remains identical. The same interior cubic scatterer inside different

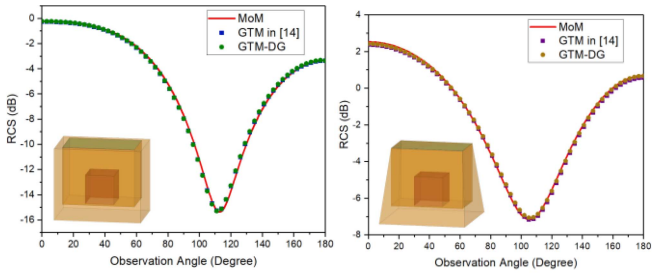

FIGURE 7. RCS of different cavities with same interior cubic scatterer. (a) Rectangular cavity (b) Pyramidal cavity.

outer surfaces is plotted in Fig. 6. Consider that an incident plane wave along the z-axis with an amplitude of 1 V/m irradiates on the cavity, and has a frequency of 150 MHz. Firstly, we study the case where the outside is a rectangular cavity and apply the mesh length of $\lambda/20$ to expand the whole surface of the cavity, so that the cavity is constructed by the conformal meshes with 430 and 298 RWGs on the external surface and internal structure, separately. The reference surface is put to describe the scattering characteristics of the internal composition and is discretized by 43 RWGs. On the view point of the DDM, the outer wall and the reference surface are two subdomains. In the case of conformal meshes, there are 16 coincident interface contours between two adjacent subdomains, so that the inner and outer transitional junction are separately expanded by 16 RWGs and 32 HRWGs.

In the DG solution, we set $\ln\Delta = -10$ at first. Fig. 7(a) illustrates the RCS results obtained by the MoM, the method in [14] and the GTM model combined with the DG method, respectively. It is obvious that the proposed GTM method has excellent agreement with the conventional MoM and previous work in [14]. This can be explained that 43 RWGs on the reference surface can validly represent the electromagnetic information of the internal composition that is expanded by 298 RWGs. Moreover, the dimension of the transition matrix in the DG-combined GTM model is the same as that in [14], both are $2N \times 2N$, where N is the number of the basis functions on the reference surface. Since HRWG basis functions are used only at the junctions, the impact on the condition number of the corresponding coefficient matrix is not significant.

To investigate the influence of the loosen coefficient Δ of (5) for the results, the value of $-\ln\Delta$ varies from 0 to 20, and the relative root mean square error is applied which can be represented as:

$$\text{Error} = 20\log(\|\mathbf{X}-\mathbf{Y}\|/\|\mathbf{Y}\|) \tag{24}$$

where $\mathbf{X}$ and $\mathbf{Y}$ can be the surface currents or the RCS results, and $\|\cdot\|$ means l_2-norm. Then we find that the currents on the exterior wall of the cavity with various values of $-\ln\Delta$ have almost the same accuracy, where their relative errors are around -57.4 dB compared with the MoM solution. In general, it is recommended to choose $\ln\Delta = 0$ for generating GTM models.

TABLE 1. Runtime for different methods.

Method	GTM Extraction Times (s)	Runtime (s)
MoM	-	114.0
GTM in [14]	24.8	67.6
GTM-DG	26.4	45.2

To verify the portability of the GTM model, we change the shape of the external region into a pyramid and keep internal structure invariant. The geometrical structure is drawn in Fig. 6.

The exterior wall is expanded by 499 RWGs and 16 HRWGs. For comparison with the method in [14], conformal meshes are used but those RWGs across the junctions are split to HRWGs. The RCS results obtained by the MoM solution, the method in [14], and the proposed method are compared in Fig. 7(b), which is in good agreement with the largest mismatch of less than 0.15 dB. Table 1 illustrates the comparison for the runtime via various methods, where the MoM is used to directly calculate the RCS, while for the proposed method because the GTM model obtained from the previous example can be reused, its runtime does not contain the GTM extraction time, which is the most efficient in this example, and the number of unknowns to be solved is much smaller than the other two methods. Moreover, in [14] the GTM model cannot be reused when dealing with the case where the jagged area of the external surface at the interface is not on the same plane as in the previous example. As here, the rectangular cavity is replaced by a pyramidal cavity, then the GTM model in [14] needs to be reprocessed, so that its runtime includes the time to re-extract the GTM model. However, the presented method directly cuts off the relationship between the external region and the internal region of the cavity. Compared with the method in [14], the overall time via the proposed method that includes the time to extract the GTM model and the time to solve the system is slightly slower because the calculation of the line-line integral and the extraction of singular points on the boundary contour are added. But it can save the cost of manually adjusting the mesh and avoid the risk of recalculating the GTM model. Therefore, no matter how the external geometry of the cavity varies, as long as the internal structure is the same, the recalculation problem can be effectively solved.

To investigate the influence of the meshing density on the extraction of the scattering properties of the interior structure, the mesh length of the exterior and interior surface of the rectangular cavity is kept as $\lambda/20$, and the mesh density is changed on the reference surface only. Then we obtain the RCS results in each case and compare them with the MoM solution in $\lambda/20$. Table 2 demonstrates some comparisons in the different number of the RWGs on the reference surface, where the relative errors of the RCS results are defined according to (24). It can be seen that as the mesh becomes

TABLE 2. Influence of the mesh density on the reference surface.

Number of RWGs	Total Times (s)	Relative Errors (dB)
16	52.5	-74.6
25	57.5	-105.3
34	62.6	-114.2
43	66.8	-131.1

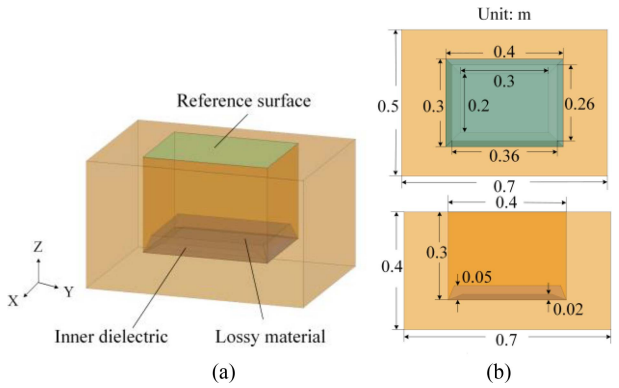

FIGURE 8. (a) The metallic cavity coated with a double-layer medium. (b) Top view and front view.

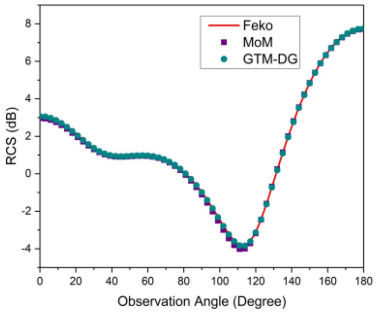

FIGURE 9. RCS of the cavity coated with a double-layer medium.

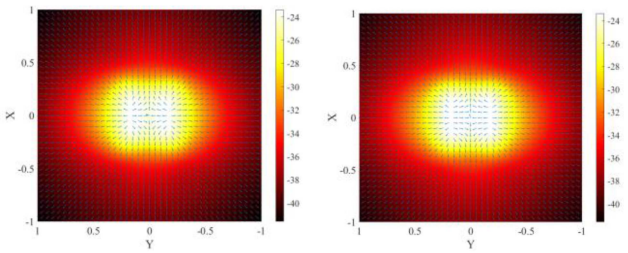

FIGURE 10. The distribution of the absolute value and direction of the Poynting vector in the finite plane with $-1 \le x \le 1$, $-1 \le y \le 1$, $z = 0.5$. (a) The MoM method (b) The GTM method.

denser, the relative errors between the two methods for calculating the scattering of the rectangular cavity decrease, which means that the ability of the GTM model to grasp the internal scattering characteristics is enhanced. In addition, the total time of operation using the MoM is 76.151s, which is larger than each case of the GTM method in Table 2.

B. CAVITY COATED WITH DIELECTRIC

The electromagnetic scattering problems of coating targets such as coated absorbing materials and plasma have received widespread attention. Stealth capability has become an important indicator for measuring the combat performance of weapons, and coating the absorbing material can reduce its RCS. The proposed method also works in dealing with coating targets.

Nano-absorbing material refers to ultra-fine material with a particle size between 1-100 nm. One of the most popular SiC lossy material currently studied can be classified as an isotropic medium. In a certain frequency band, the medium parameters are $\varepsilon_r = 8.0 - j3.5$, $\mu_r = 1$. We apply a metallic cavity coated with a double-layer medium. Firstly, the bottom wall of the cavity is coated with a medium whose relative permittivity is 4. Then the lossy materials are coated thereon. The model of a complex cavity with double-layer coated media is analyzed in Fig. 8(a) and the details of the coated dielectric are drawn in Fig. 8(b). On both sides of the double-layer medium, smooth surfaces are transitioning to connect with the metal wall of the cavity. The operating frequency is 300 MHz and the incident wave is still along the z-axis.

Inside the cavity, the DG method is applied to deal with the discontinuity of current between the planes. Adopting DDM as mentioned in Section II-B, we consider the two layers of different media, the metal area covered by the media, and the inner uncoated surface of the cavity as different subdomains. Within the subdomain, the RWG basis functions are defined for the discretization of electric and magnetic currents. While on the boundary portion, the HRWG basis functions are used. In this way, when only a small number of unknowns is added, the continuity of the current can be cut off to ensure computational accuracy. In addition, the dielectric and the internal metal surface are regarded as different boundary conditions, and the rest of derivations is basically identical.

The exterior surface and reference surface are discretized by 924 and 97 RWGs. The internal and external layers of the dielectric are expanded by 130 RWGs and 28 HRWGs, 181 RWGs and 28 HRWGs respectively. Moreover, there are 97 RWGs and 22 HRWGs expanded on the surface coated by the media, and 372 RWGs and 22 HRWGs defined in the uncoated inner area. That is, there are a total of 780 RWGs and 100 HRWGs in the interior region, while there are only 97 RWGs on the reference surface.

In this way, the total number of unknowns in the system is much less than that required by the traditional MoM method. The scattering results obtained by Altair FEKO 2017, MoM and the GTM models are shown in Fig. 9 with satisfactory accuracy. Moreover, we select a finite plane with $-1 \le x \le 1$, $-1 \le y \le 1$, $z = 0.5$ and sample on the surface to calculate the absolute value and direction of the Poynting vector at each point, which is compared with results obtained by the MoM in Fig. 10. It can be seen that the distributions of the Poynting vector are similar without noticeable differences between the two results. Therefore, the electromagnetic information of the complex double-layer coated

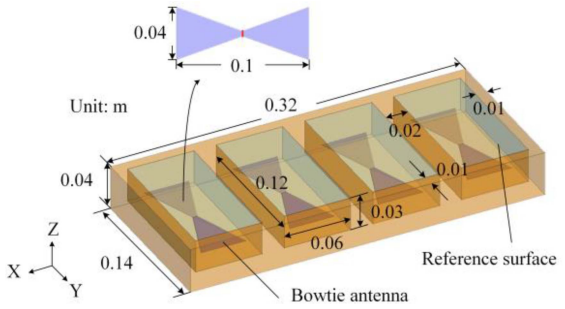

FIGURE 11. A metallic block with four identical cavities, where a bowtie antenna is placed inside each cavity.

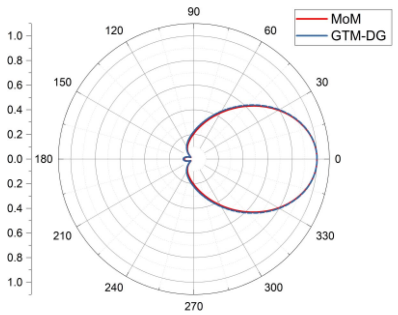

FIGURE 12. Normalized Radiation patterns of antennas in the H plane at 1.5 GHz.

medium structure inside the cavity can be accurately mapped onto the reference surface.

C. PERIODIC CAVITY ARRAY STRUCTURE

For the periodic cavity array, the GTM model only needs to be calculated once and the other cavities can apply this GTM model repeatedly. With the help of the DG method, it is needless to consider the outer shape of the cavity and the meshing situation when reusing the GTM model. Besides, if two modules in the system have the same relative displacement, their field transmission matrices are the same [26]. Hence, the GTM method is suitable for processing the periodic cavity system.

A metallic block with four identical cavities is plotted in Fig. 11, where a bowtie antenna is placed inside each cavity. Without the exterior incident wave, the system operates under the interior source only at the feeding point of the bowtie antenna. All the cavities share the same exterior wall of the metallic block. This periodic cavity structure can be used both as a reflector of an antenna and as isolation between ports. The details of the bowtie antenna are also shown in Fig. 11. The delta-gap voltage source is loaded on the feed line. The operating frequency is set to 1.5 GHz.

One GTM reference surface is expanded by 225 RWGs and 36 HRWGs. To be able to reuse this GTM model in all cavities of the metallic block, we force the triangular meshes on each reference surface to keep identical. The interior surface and the bowtie antenna of each cavity is discretized into 748 RWGs, and the outer surface is expanded by 2214 RWGs and 120 HRWGs.

From Fig. 12, it is clear that the normalized directivity (*xoz* plane) of the H-plane at 1.5 GHz calculated by the GTM method is consistent with the result obtained by the MoM. It is seen that the scattering of the interior ingredients represented by 748 RWGs is extracted by the GTM model discretized into 225 RWGs in effect. Under the excitation of the delta-gap voltage source, the induced current inside the cavity is extracted onto the reference surface in the form of a rotated tangential component. That is, the GTM model conveys the radiation information about the internal voltage excitation.

Table 3 lists some comparisons between the MoM and the GTM method. The total quantity of unknowns in this periodic cavity system by the proposed method is 56.8% of the number of unknowns needed in the conventional MoM. Moreover, the proposed method takes a total of 1443.68s, including the time to obtain the GTM model and the time to solve the multi-cavities system. It saves 66.27% of the time compared with the MoM. It can be expected that as the quantity of the periodic cavities rises, the GTM method will be more rapid and efficient than the MoM because the GTM model can be directly reused to those additive cavities.

In the problem of the multi-cavities system, the information between different cavities is transmitted to each other through the reference surface in the GTM model, instead of the direct coupling in the conventional method. Therefore, in analyzing the coupling effect of the complex array system, with the use of the DG method, the calculation efficiency and the applicable range of the proposed method have been greatly improved.

D. AIRCRAFT INLET WITH MULTI-WINDOWS

In this section, we show an aircraft inlet model. The aircraft inlet is a typical cavity structure. After multiple reflections of the radar wave in the inlet, it is one of the main strong scattering sources for the forward direction of the aircraft. The aircraft inlet has an air inlet and an air outlet so that it can be considered as a promotion form of the cavity with multi-windows.

Consider a simple model of an aircraft inlet with turbine blades and connecting devices plotted in Fig. 13(a). The details of the model are shown in Fig. 13(b) and (c). The overall length is 6.5 m and the wall thickness is 0.2 m. The right elliptical inlet has a long axis of 1.3 m and a short axis of 0.65 m. The left circular inlet has a radius of 1.5 m and the arc length of the turbine blades is 2.8 m. Besides, the connecting shaft is 0.15 m. The interior and exterior planes of the pipeline model are spline surfaces.

Although the turbine blades are located inside the inlet port, since the blades and the rotating shaft will rotate under the operating state, the condition required by the GTM method that the inner structure of the cavity does not change is not satisfied. Therefore, we place the left reference surface on the connecting shaft and put the turbine outside the

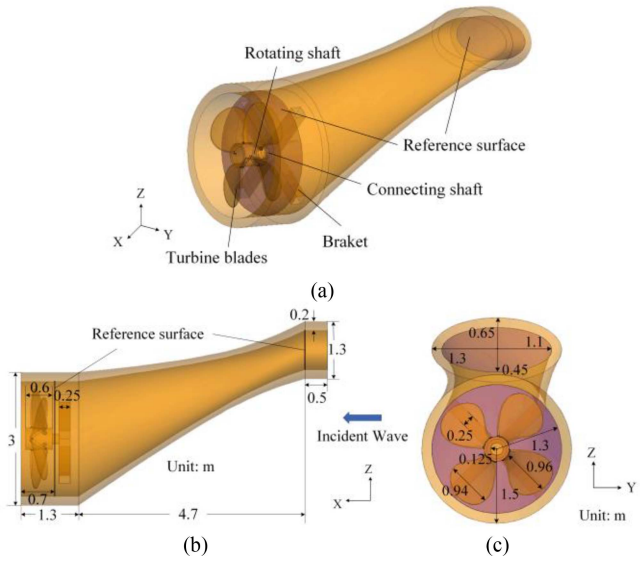

FIGURE 13. (a) The aircraft inlet model. (b) The geometrical size of the cavity at the front view. (c) The geometrical size of the cavity at the left view.

TABLE 3. Comparison for different methods.

Method	GTM Extraction Times (s)	Total Time (s)	The Number of Unknowns
MoM	-	4280.5	5886
GTM	175.6	1443.7	3343

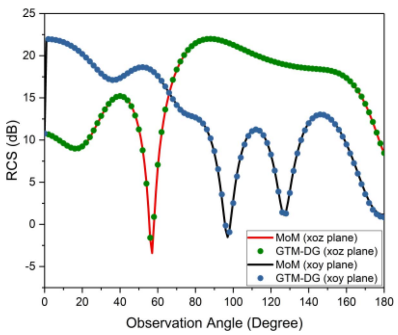

FIGURE 14. RCS of the aircraft inlet model in the *xoz* plane and *xoy* plane.

reference surface as a part of the exterior region. The right reference surface is set to close the elliptical inlet. Moreover, the model is irradiated by an incident plane wave of 80 MHz along x-axis.

We regard two reference surfaces as a whole which are meshed by 331 RWGs and 52 HRWGs. The exterior wall of the cavity containing turbine blades and the partial connecting shaft is discretized by 12342 RWGs and 81 HRWGs. The inner structure including the turbine bracket is constructed by 6928 RWGs.

Fig. 14 compares the RCS results of the model obtained by both conventional MoM and the GTM method. It is attractive that the results calculated by the GTM method are practically almost identical to the reference solution in both *xoz* plane and *xoy* plane. The traditional method requires calculating the impedance matrix of the entire system when the blade is rotated by a certain angle. As for the proposed method, the reference surface separates the system into a dynamic area and static area. When calculating the scattering problem of the entire system, it is only necessary to update the impedance information of the dynamic area, which can reduce much complexity with the fine structure inside the static area.

Once the GTM model is obtained, with a combination of the DG method we can easily transplant it into the same inlet model of different aircrafts. Not limited to the inlet, the proposed GTM method can be applied to solve the scattering problem of porous cavities and accurately describe the radiation information of the interior region of the cavity.

Although MoM is used in the proposed formulation, it is worth noting that other methods can also be applied to map the electromagnetic scattering characteristics of the internal structure onto the reference surface. For example, the mode matching method may be more efficient for long cavities with cascaded regular waveguides.

IV. CONCLUSION

In this paper, a GTM model combined with the DG method is presented for dealing with the scattering properties of open-ended cavities. An artificial reference surface is put to seal the cavity into the surface-perfect structure and separate the cavity into an exterior dynamic region and interior static region. The GTM model can precisely capture the radiation and scattering characteristic of the interior ingredient of the cavity. Applying the DG method based on DDM makes it convenient to transplant the GTM model into different exterior environments, even into rotating environments, as long as the inner region of the cavity keeps identical. Meanwhile, with the help of nonconformal mesh, the control of mesh density in different regions can be realized. Numerical examples demonstrate the high feasibility and excellent precision of the presented GTM method under the conditions of both conformal and nonconformal meshes.

REFERENCES

[1] X. Di, A. W. Glisson, and K. A. Michalski, "Analysis of a dielectric resonator antenna in a cylindrical conducting cavity: HEM modes," *IEE Proc. Microw. Antennas Propag.*, vol. 141, no.1, pp. 8–14, Feb. 1994.

[2] Z. Zhang *et al.*, "Triple-mode dielectric-loaded cylindrical cavity diplexer using novel packaging technique for LTE base-station applications," *IEEE Trans. Compon. Packag. Manuf. Technol.*, vol. 6, no. 3, pp. 383–389, Mar. 2016.

[3] Q. Li and Y. Zhang, "Analytical solutions and characteristics for shielded asymmetrical coplanar stripline and its transition to rectangular waveguide," *IEEE Trans. Microw. Theory Techn.*, vol. 66, no. 5, pp. 2090–2099, May 2018.

[4] A. W. Glisson and D. R. Wilton, "Simple and efficient numerical methods for problems of electromagnetic radiation and scattering from surfaces," *IEEE Trans. Antennas Propag.*, vol. 28, no. 5, pp. 593–603, Sep. 1980.

[5] K. R. Umashankar, A. Taflove, and S. M. Rao, "Electromagnetic scattering by arbitrary shaped three-dimensional homogeneous lossy dielectric objects," *IEEE Trans. Antennas Propag.*, vol. 34, no. 6, pp. 758–766, Jun. 1986.

[6] J. Liu and J.-M. Jin, "A special higher order finite-element method for scattering by deep cavities," *IEEE Trans. Antennas Propag.*, vol. 48, no. 5, pp. 694–703, May 2000.
[7] T. T. Chia, J. Burkholder, and R. Lee, "The application of FDTD in hybrid methods for cavity scattering analysis," *IEEE Trans. Antennas Propag.*, vol. 43, no. 10, pp. 1082–1090, Oct. 1995.
[8] D. C. Ross, J. L. Volakis, and H. Hannastassiu, "Hybrid finite element-modal analysis of jet engine inlet scattering," *IEEE Trans. Antennas Propag.*, vol. 43, no. 3, pp. 277–285, Mar. 1995.
[9] A. Barka, P. Soudais, and D. Volpert, "Scattering from 3-D cavities with a plug and play numerical scheme combining IE, PDE, and modal techniques," *IEEE Trans. Antennas Propag.*, vol. 48, no. 5, pp. 704–712, May 2000.
[10] P. Li and L. J. Jiang, "Modeling radiated emissions through shielding boxes based on the tangential electrical field samplings over openings," *IEEE Trans. Electromagn. Compat.*, vol. 55, no. 6, pp. 1140–1146, Dec. 2013.
[11] T. Van and A. W. Wood, "A time-domain finite element method for Helmholtz equations," *J. Comput. Phys.*, vol. 183, no. 2, pp. 486–507, Dec. 2002.
[12] R. Uber and A. Wood, "Finite-element boundary integral simulation of transient electromagnetic scattering from multiple cavities," *IEEE Trans. Antennas Propag.*, vol. 65, no. 6, pp. 3267–3272, Jun. 2017.
[13] M. Li and W. C. Chew, "Wave-field interaction with complex structures using equivalence principle algorithm," *IEEE Trans. Antennas Propag.*, vol. 55, no. 1, pp. 130–138, Jan. 2007.
[14] S. Xiang, G. Xiao, and J. Mao, "A generalized transition matrix model for open-ended cavity with complex internal structures," *IEEE Trans. Antennas Propag.*, vol. 64, no. 9, pp. 3920–3930, Sep. 2016.
[15] G. Xiao, J. Mao, and B. Yuan, "Generalized transition matrix for arbitrarily shaped scatterers or scatterer groups," *IEEE Trans. Antennas Propag.*, vol. 56, no. 12, pp. 3723–3732, Dec. 2008.
[16] S. M. Rao, D. R. Wilton, and A. W. Glisson, "Electromagnetic scattering by surfaces of arbitrary shape," *IEEE Trans. Antennas Propag.*, vol. 30, no. 3, pp. 409–418, May 1982.
[17] B. Cockburn, G. E. Karniadakis, and C.-W. Shu, *Discontinuous Galerkin Methods: Theory, Computation and Applications*. Tokyo, Japan: Springer, 2000.
[18] J. Hesthaven and T. Warburton, *Nodal Discontinuous Galerkin Methods*. New York, NY, USA: Springer, 2008.
[19] Z. Peng, K.-H. Lee, and J.-F. Lee, "A discontinuous Galerkin surface integral equation method for electromagnetic wave scattering from nonpenetrable targets," *IEEE Trans. Antennas Propag.*, vol. 61, no. 7, pp. 3617–3628, Jul. 2013.
[20] G. Xiao and Y. Hou, "Intuitive formulation of discontinuous Galerkin surface integral equations for electromagnetic scattering problems," *IEEE Trans. Antennas Propag.*, vol. 65, no. 1, pp. 287–294, Jan. 2017.
[21] M. A. E. Bautista, F. Vipiana, M. A. Francavilla, J. A. T. Vasquez, and G. Vecchi, "A nonconformal domain decomposition scheme for the analysis of multiscale structures," *IEEE Trans. Antennas Propag.*, vol. 63, no. 8, pp. 3548–3560, Aug. 2015.
[22] Z. Peng, R. Hiptmair, Y. Shao, and B. MacKie-Mason, "Domain decomposition preconditioning for surface integral equations in solving challenging electromagnetic scattering problems," *IEEE Trans. Antennas Propag.*, vol. 64, no. 1, pp. 210–223, Jan. 2016.
[23] B. Kong and X. Sheng, "A discontinuous Galerkin surface integral equation method for scattering from multiscale homogeneous objects," *IEEE Trans. Antennas Propag.*, vol. 66, no. 4, pp. 1937–1946, Apr. 2018.
[24] B. Kong, Y. Ylä-Oijala, and A. Sihvola, "A discontinuous Galerkin surface integral equation method for scattering from IBC targets," *Int J. Numer. Model. Elect. Netw. Devices Fields*, vol. 33, p. e2650, Jul. 2019.
[25] Y. Hu, R. Liu, S. Xiang, and G. Xiao, "Generalized transition matrix models for open cavities," in *Proc. Photon. Electromagn. Res. Symp. Fall (PIERS - Fall)*, Xiamen, China, Dec. 2019, pp. 1901–1907.
[26] S. Xiang, G. Xiao, X. Tian, and J. Mao, "Analysis of large-scale phased antenna array with generalized transition matrix," *IEEE Trans. Antennas Propag.*, vol. 61, no. 11, pp. 5453–5464, Nov. 2013.

YUYANG HU (Graduate Student Member, IEEE) received the B.S. degree in telecommunications engineering from Xidian University, Xi'an, China, in 2018. He is currently pursuing the Ph.D. degree with the Key Laboratory of Ministry of Education of Design and Electromagnetic Compatibility of High Speed Electronic Systems, Shanghai Jiao Tong University, Shanghai.

His current research interests include computational electromagnetics and its application in scattering and radiation problems.

GAOBIAO XIAO (Member, IEEE) received the B.S. degree from the Huazhong University of Science and Technology, Wuhan, China, in 1988, the M.S. degree from the National University of Defense Technology, Changsha, China, in 1991, and the Ph.D. degree from Chiba University, Chiba, Japan, in 2002.

He has been a faculty member with the Department of Electronic Engineering, Shanghai Jiao Tong University, Shanghai, China, since 2004. His research interests are computational electromagnetics, coupled thermo-electromagnetic analysis, microwave filter designs, fiber-optic filter designs, phased arrays, and inverse scattering problems.

SHANG XIANG (Member, IEEE) received the Ph.D. degree from Shanghai Jiao Tong University, Shanghai, in 2016.

He is currently a Postdoctoral Researcher with the Department of Electrical and Information Technology, Lund University. His research interests include computational electromagnetics, massive MIMO antenna, theory of characteristic modes, and reconfigurable metasurface reflectarray.